

Development of $\text{Li}(\text{Ni}_{1/3}\text{Mn}_{1/3}\text{Co}_{1/3-x}\text{Na}_x)\text{O}_2$ cathode materials by synthesizing with glycine nitrate combustion technique for Li-ion rechargeable batteries

T. H. N. G. Amaraweera^{1,2} · Athula Wijayasinghe¹ · B.-E. Mellander³ · M. A. K. L. Dissanayake¹

Received: 9 November 2016 / Revised: 26 March 2017 / Accepted: 4 April 2017
© Springer-Verlag Berlin Heidelberg 2017

Abstract Glycine nitrate combustion technique was investigated for synthesizing $\text{Li}(\text{Ni}_{1/3}\text{Mn}_{1/3}\text{Co}_{1/3-x}\text{Na}_x)\text{O}_2$, $x = 0-0.11$ based transition metal oxide cathode materials for the rechargeable Li-ion battery (LIB) under this study. X-ray diffraction and scanning electron microscopy analysis showed that the synthesized powder samples were well crystalline rather spherical secondary particles. These secondary particles were composed of softly agglomerated nano-scale primary particles. The room temperature electrical conductivity of these Na-doped materials was significantly higher than that of the base material (2.60×10^{-7} S/cm). Among them, the $x = 0.04$ material reported the highest electrical conductivity of 1.02×10^{-03} S cm^{-1} . The half-cell assembled with cathode fabricated from $\text{Li}(\text{Ni}_{1/3}\text{Mn}_{1/3}\text{Co}_{1/3})\text{O}_2$ base material showed an initial discharge capacity of $187 \text{ mA h}^{-1} \text{ g}^{-1}$ with $25 \text{ mA h}^{-1} \text{ g}^{-1}$ irreversible capacity loss and 88.47% columbic efficiency at C/5 rate with a cut-off voltage of 2.5–4.6 V at 25 °C. The electrochemical behavior of the $x = 0.04$ cathode showed a comparable initial discharge capacity as of the base material but with improved capacity retention.

Keywords Lithium ion rechargeable battery · Cathode material · Transition metal oxide · Glycine nitrate combustion method · Cell performance

✉ Athula Wijayasinghe
athula@ifs.ac.lk

¹ National Institute of Fundamental Studies, Hantana Road, Kandy, Sri Lanka

² Department of Science and Technology, Uva Wellassa University, Badulla, Sri Lanka

³ Department of Physics, Chalmers University of Technology, Göteborg, Sweden

Introduction

General background

Rechargeable lithium-ion batteries (LIB) have now emerged as the preferred power sources for portable electronic devices and specially for electric vehicles, mainly because of their high volumetric and gravimetric energy densities. A majority of commercially available lithium ion batteries uses lithiated transition metal oxide such as LiCoO_2 , LiFePO_4 , and LiMn_2O_4 as the cathode material. Recently, the layered $\text{Li}(\text{Ni}_{1/3}\text{Mn}_{1/3}\text{Co}_{1/3})\text{O}_2$ has been investigated extensively as an alternative cathode material because of its favorable features such as high capacity, structural stability, thermal stability, low cost, and safety [1, 2]. This material with a theoretical capacity of 278 mAh g^{-1} has been shown to deliver $150 \text{ h}^{-1} \text{ g}^{-1}$ cycled between 2.5 and 4.2 V and close to $200 \text{ mA h}^{-1} \text{ g}^{-1}$ when charged to 4.6 V [1–5]. Tetravalent Mn in $\text{Li}(\text{Ni}_{1/3}\text{Mn}_{1/3}\text{Co}_{1/3})\text{O}_2$ is electrochemically inactive and plays an important role of supporting the host structure during Li^+ de-intercalation resulting structural stability [2]. Time-resolved X-ray diffraction in a wide temperature range from 25 to 600 °C implies that the initial layer structure changes first to a LiM_2O_4 type spinel in a temperature range from 236 to 350 °C, and then to M_3O_4 -type spinel from 350 to 441 °C, and remains this structure up to 600 °C [1, 6]. However, high irreversible capacity during the first cycle and poor long-term cycling behavior are some disadvantages of $\text{Li}(\text{Ni}_{1/3}\text{Mn}_{1/3}\text{Co}_{1/3})\text{O}_2$ [3–5].

Recent studies show an improvement in rate capabilities in nanostructured $\text{Li}(\text{Ni}_{1/3}\text{Mn}_{1/3}\text{Co}_{1/3})\text{O}_2$ electrode materials [7, 8]. This was attributed to increased electrochemically active surface due to the combined effect of smaller particle size and higher internal porosity [6]. However, nanosized particles can be harmful for battery applications because of their high

reactivity with the electrolyte [4]. Therefore, sub-micron size $\text{Li}(\text{Ni}_{1/3}\text{Mn}_{1/3}\text{Co}_{1/3})\text{O}_2$ particles with primary nano-scale particles can be desirable as they can be more chemically stable than the nano-size particles and possess a greater rate capability than the micron size particles due to its high active surface area compared to volume [8].

Substitution of Na for Li in three component layered transition metal oxides of Ni, Mn, and Co (NMC) has been identified as an effective method to improve the electrochemical performance recently [3, 9]. The ionic radii of Na^+ (1.02 Å) is considerably larger than that of Li^+ (0.76 Å), which may increase the interlayer space and make the intercalation and deintercalation of lithium faster. Moreover, it is expected that doping of Na into the NMC oxides may activate the reduction process of Mn^{4+} to Mn^{3+} after initial charge providing additional vacancies for Li insertion with higher discharge capacity [9]. For example, Na-doped $\text{Li}_{0.95}\text{Na}_{0.05}\text{Ni}_{1/3}\text{Co}_{1/3}\text{Mn}_{1/3}\text{O}_2$ was synthesized by hydroxide co-precipitation. This electrode material shows higher initial discharge capacity under current density of 27 mA g^{-1} ($250.5 \text{ mA h}^{-1} \text{ g}^{-1}$) and better electrochemical performance than $\text{Li}(\text{Ni}_{1/3}\text{Mn}_{1/3}\text{Co}_{1/3})\text{O}_2$ ($155.4 \text{ mA h}^{-1} \text{ g}^{-1}$) in the potential range of 2.0–4.5 V [3]. Na-substituted $\text{Li}_{1-x}\text{Na}_x(\text{Ni}_{1/3}\text{Mn}_{1/3}\text{Co}_{1/3})\text{O}_2$ material synthesized by molten salts method showed initial discharge capacity of $175.8 \text{ mA h}^{-1} \text{ g}^{-1}$ for $x = 0.00$, $174.0 \text{ mA h}^{-1} \text{ g}^{-1}$ for $x = 0.001$, $170.9 \text{ mA h}^{-1} \text{ g}^{-1}$ for $x = 0.01$, $172.7 \text{ mA h}^{-1} \text{ g}^{-1}$ for $x = 0.03$ and $166.5 \text{ mA h}^{-1} \text{ g}^{-1}$ for $x = 0.05$ between 2.7 and 4.4 V under current density of 16 mA g^{-1} [10]. Na-substituted $\text{Li}_{1-x}\text{Na}_x(\text{Ni}_{1/3}\text{Mn}_{1/3}\text{Co}_{1/3})\text{O}_2$ materials also showed improved rate capability and cycling performances compared to pure $\text{Li}(\text{Ni}_{1/3}\text{Mn}_{1/3}\text{Co}_{1/3})\text{O}_2$ [10]. Study based on $\text{Li}_{1.2-x}\text{Na}_x(\text{Ni}_{0.13}\text{Co}_{1.3}\text{Mn}_{0.54})\text{O}_2$ material synthesized by simple polymer-pyrolysis method delivers higher discharge capacity ($307 \text{ mA h}^{-1} \text{ g}^{-1}$), improved rate capability ($139 \text{ mA h}^{-1} \text{ g}^{-1}$ at 8C, and cycling stability (89% capacity retention after 100 cycles) than $\text{Li}_{1.2}(\text{Ni}_{0.13}\text{Co}_{1.3}\text{Mn}_{0.54})\text{O}_2$ electrode within a voltage range of 2.0–4.8 V vs. Li^+/Li [11]. However, the effect of Na addition to $\text{Li}(\text{Ni}_{1/3}\text{Mn}_{1/3}\text{Co}_{1/3})\text{O}_2$ has not adequately been investigated.

Material synthesis by the glycine nitrate combustion technique

The synthesis route employed will deeply affect the morphology and particle size, which govern the electrochemical performance of the cathode material [7, 12]. Traditionally, the cathode active materials are prepared by solid state methods and wet chemical routes [8, 13–15]. Furthermore, combustion methods have also been successfully used to synthesize cathode materials. Among the combustion synthesis methods, glycine nitrate combustion (GNC) is a self-sustaining combustion process which uses a metal nitrate as the oxidizer and glycine

as the fuel [15–18]. Further, glycine, is known as a complexing agent for a number of metal ions [17]. In this GNC synthesis process, the vigorous gas evolution from the combustion reaction often produces highly open, nanostructured powders. Wet chemical routes such as hydroxide co-precipitation and molten salts method were employed to synthesize Na-substituted $\text{Li}_{1-x}\text{Na}_x(\text{Ni}_{1/3}\text{Mn}_{1/3}\text{Co}_{1/3})\text{O}_2$ materials [3, 9–11]. However, GNC synthesis process was not used to synthesize Na-substituted $\text{Li}(\text{Ni}_{1/3}\text{Mn}_{1/3}\text{Co}_{1/3})\text{O}_2$. Hence, this study was devoted to explore the Na-doped $\text{Li}(\text{Ni}_{1/3}\text{Mn}_{1/3}\text{Co}_{1/3})\text{O}_2$ base material system by investigating novel $\text{Li}(\text{Ni}_{1/3}\text{Mn}_{1/3}\text{Co}_{1/3-x}\text{Na}_x)\text{O}_2$, $x = 0\text{--}1.1$, materials synthesized by GNC process.

Experimental

Powder synthesis by the glycine nitrate combustion method

$\text{Li}(\text{Ni}_{1/3}\text{Mn}_{1/3}\text{Co}_{1/3-x}\text{Na}_x)\text{O}_2$ -based oxide powders were synthesized by the glycine nitrate combustion (GNC) method while keeping the glycine: nitrate as 0.6 [15–18]. For that, stoichiometric amounts of metal nitrates, LiNO_3 , $\text{Ni}(\text{NO}_3)_2 \cdot 6\text{H}_2\text{O}$, $\text{Co}(\text{NO}_3)_2 \cdot 6\text{H}_2\text{O}$, $\text{Mn}(\text{NO}_3)_2 \cdot 4\text{H}_2\text{O}$, and NaNO_3 (Merck, Germany) were added to distilled water. The precursor solution was then thoroughly mixed using a magnetic stirrer hotplate at room temperature for 2 h. Then, it was mixed at 60°C for 1 h and at 100°C another 1 h. Then, the solution temperature was increased stepwise (25°C) from 100 to 300°C . As the temperature increases, dark violet color foam was formed. Combustible gases such as N_2O , NH_3 , and CO_2 were observed liberating as the heating continued, and the process of heating was continued further [16–19]. Then, exothermic decomposition began due to the possible heat disintegration reaction of glycine accompanied by the evolution of volatile combustible gases eventually resulting in an ash product. Finally, the ash product was calcinated at 900°C in air for 2 h to obtain the final oxide powder. While cooling down after the calcination, the powders were kept at 800°C for 1 h.

Powder characterization

X-ray diffraction (XRD, Siemens D5000) using $\text{CuK}\alpha$ radiation was used to phase analysis, and the scanning electron microscopy (SEM, FEI Quanta 200 FEG-ESEM) was employed to study the particle size and morphology of the synthesized powder. Thermogravimetric analyses (TGA) were performed using a Perkin-Elmer TGS-2 Thermogravimetric System by heating the synthesized powders up to 800°C in a platinum pan at a rate of 5°C min^{-1} under nitrogen atmosphere.

Powder densification and electrical characterization

Solid pellets of 12 mm diameter and 0.5 mm in length were pressed by cold uni-axially at 200 MPa and subsequently sintered at 1000 °C for 2 h in air. For the conductivity measurements, first, the flat end surfaces of the sintered pellets were pasted with a thin layer of the gold paste (G3535, Agar Scientific Ltd., England). After allowing to drying, the pasted pellets were kept in a box furnace (brand) and heat treated at 750 °C for 2 h in air. The idea behind this gold pasting was to improve the contacts between the specimen pellets and the platinum electrodes of the sample holder. The d.c. four probe electrical conductivity measurements were performed on these prepared pellets in the temperature range between 25 and 200 °C.

Electrochemical characterization

For electrochemical characterization, electrodes were prepared using the slurry containing 85 wt% of the prepared $\text{Li}(\text{Ni}_{1/3}\text{Mn}_{1/3}\text{Co}_{1/3-x}\text{Na}_x)\text{O}_2$ active material with 5 wt% carbon black (Sigma-Aldrich) and 10 wt% PVDF (KynarFlex 2801) in Acetone (Sigma-Aldrich). The prepared slurry was then manually tape cast onto an aluminum-foil by the doctor blade method. After drying, circular disks electrodes were cut from the fabricated tapes.

Coin cells (Type CR 2032) were assembled in an argon-filled glove-box (<1 ppm O_2 and H_2O) with the developed cathode electrodes, Li-foil (Sigma-Aldrich) as the reference and counter electrodes and Cellgard 2400 as the separator and the non-aqueous electrolyte of 1 M LiPF_6 in ethylene carbonate (EC)/diethyl carbonate (DEC)/dimethyl carbonate (DMC) (1:1:1 wt%) (Selectlyte LP71, BASF, USA). Finally, the charge-discharge study of assembled cells was carried out at C/5 rate with a cut-off voltage of 2.5–4.6 V at 25 °C using Scribner 580 Battery Testing System controlled by BCycle 2.0 program.

Results and discussion

$\text{Li}(\text{Ni}_{1/3}\text{Mn}_{1/3}\text{Co}_{1/3-x}\text{Na}_x)\text{O}_2$, $x = 0.00, 0.04, 0.08$, and 0.11 synthesized by GNC method

Figure 1 shows the X-ray diffractograms obtained on $\text{Li}(\text{Ni}_{1/3}\text{Mn}_{1/3}\text{Co}_{1/3-x}\text{Na}_x)\text{O}_2$, $x = 0.00, 0.04, 0.08$, and 0.11 materials prepared in this study. In this figure, existence of the appropriate R3m phase of $\alpha\text{-NaFeO}_2$ layered structure of $\text{Li}(\text{Ni}_{1/3}\text{Co}_{1/3}\text{Mn}_{1/3})\text{O}_2$ phase can be seen in all these powder samples [2].

In order to study the effect of Na addition to the $\text{Li}(\text{Ni}_{1/3}\text{Mn}_{1/3}\text{Co}_{1/3})\text{O}_2$ base material, where Co is partially

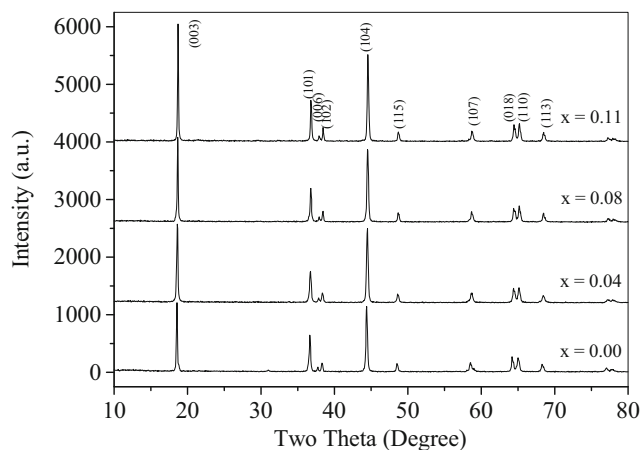


Fig. 1 X-ray diffractograms of $\text{Li}(\text{Ni}_{1/3}\text{Mn}_{1/3}\text{Co}_{1/3-x}\text{Na}_x)\text{O}_2$, $x = 0.00, 0.04, 0.08$, and 0.11 materials

substituted by Na, the $\text{Li}(\text{Ni}_{1/3}\text{Mn}_{1/3}\text{Co}_{1/3-x}\text{Na}_x)\text{O}_2$, $x = 0.04, 0.08$, and 0.11 compositions were synthesized and characterized. The X-ray diffractograms obtained for the $\text{Li}(\text{Ni}_{1/3}\text{Mn}_{1/3}\text{Co}_{1/3-x}\text{Na}_x)\text{O}_2$, $x = 0.00, 0.04, 0.08, 0.11$ materials prepared in this study are also presented in Fig. 1. In all these diffractograms, the peaks are sharp and well-defined, suggesting that the materials are well crystallized. These diffraction peaks could be indexed on the basis of a hexagonal structure of $\alpha\text{-NaFeO}_2$ (space group R3m) [3]. No traces for secondary phases can be seen in these XRD patterns, indicating phase pure materials [3]. Further, clear splitting of the (006) and (102) as well as (108) and (110) diffraction peaks indicates an orderly distributed lithium and transition-metal ions in the structure as explained elsewhere [17]. This may result due to the ability of GNC synthesis process to homogeneously mix metal ions at the atomic scale.

The lattice parameters, a and c of the prepared $\text{Li}(\text{Ni}_{1/3}\text{Mn}_{1/3}\text{Co}_{1/3-x}\text{Na}_x)\text{O}_2$ materials, are given in Table 1. Accordingly, the lattice parameter c and the ratio c/a increase with Na^+ content from $x = 0$ to 0.04 . This behavior suggests that Na^+ (1.02 Å) has been well substituted for $\text{Li}(\text{Ni}_{1/3}\text{Mn}_{1/3}\text{Co}_{1/3-x}\text{Na}_x)\text{O}_2$ resulting uniform solid solution [3]. Further, the increase in c -parameter provides a direct evidence of the expansion of the Li layer, which is beneficial for

Table 1 Variation of lattice parameters a , c , c/a , and electrical conductivity of the prepared $\text{Li}(\text{Ni}_{1/3}\text{Mn}_{1/3}\text{Co}_{1/3-x}\text{Na}_x)\text{O}_2$ materials

x in $\text{Li}(\text{Ni}_{1/3}\text{Mn}_{1/3}\text{Co}_{1/3-x}\text{Na}_x)\text{O}_2$	a (Å)	c (Å)	c/a	$I(003)/I(104)$	Electrical conductivity (S cm^{-1})
0.00	2.8712	14.2781	4.9728	1.0587	2.06×10^{-7}
0.04	2.8589	14.3112	5.0057	1.0562	1.02×10^{-3}
0.08	2.8626	14.2732	4.9860	1.1681	7.98×10^{-5}
0.11	2.8618	14.2354	4.9743	1.3518	8.61×10^{-5}

the Li^+ diffusion between oxygen layers [3]. The c/a value of $\text{Li}(\text{Ni}_{1/3}\text{Mn}_{1/3}\text{Co}_{1/3-0.04}\text{Na}_{0.04})\text{O}_2$ is higher than that of $\text{Li}(\text{Ni}_{1/3}\text{Mn}_{1/3}\text{Co}_{1/3})\text{O}_2$ indicating a reduction in the degree of cation mixing due to reduction of Ni^{+2} in Li layer with the occupation of Na^+ [3].

Further, this XRD study indicates that during the substitution of larger Na^+ (1.02 Å) for smaller Li^+ (0.76 Å), from $x = 0.08$ to $x = 0.11$, the c lattice parameter has decreased from 14.2732 to 14.2354. Qiu et al. reported that the excessive Na^+ leads to the formation of impure $\text{Na}_{0.7}\text{MnO}_{2+\alpha}$ phase when the Na^+ content passes its limit in the host structure and this was inferred from the observed reduction of lattice parameter [8]. However, no impurity phases can be seen in the XRD pattern of $\text{Li}(\text{Ni}_{1/3}\text{Mn}_{1/3}\text{Co}_{1/3-x}\text{Na}_x)\text{O}_2$, $x = 0.08$ and 0.11 materials prepared in the present study, as given in Fig. 1.

Figure 2 shows the SEM images obtained on $\text{Li}(\text{Ni}_{1/3}\text{Mn}_{1/3}\text{Co}_{1/3-x}\text{Na}_x)\text{O}_2$, $x = 0.00, 0.04, 0.08$, and 0.11 materials. The SEM images indicate that all the powder samples comprise of well crystallized particles. Rather, quasi-

spherical particles with two different particle sizes can be clearly identified in all these materials. The bigger secondary particles are seen as soft agglomerates of the size of few microns formed by agglomerating nano-scale primary particles. These primary particles are rather spherical in shape, with particle size in the nano-scale. The primary particles of $\text{Li}(\text{Ni}_{1/3}\text{Mn}_{1/3}\text{Co}_{1/3-x}\text{Na}_x)\text{O}_2$, $x = 0.00$ are characterized by uniform sizes (~200 nm). In contrast, somewhat spherical primary particles with two different particle sizes (400–1000 and 100–300 nm) can be clearly identified from the Na-doped $\text{Li}(\text{Ni}_{1/3}\text{Mn}_{1/3}\text{Co}_{1/3-x}\text{Na}_x)\text{O}_2$, $x = 0.00, 0.04, 0.08$, and 0.11 materials. Furthermore, size of the primary particles increases with the increasing level of Na substitution. This kind of morphology that is sub-micron size secondary particles composed with primary nano-scale particles can enhance the electrochemical performance of a material. Firstly, the higher surface area resulting from nano-scale primary particles provides more active sites for the necessary electrochemical reactions without decreasing the tapping density [8, 12]. The submicron

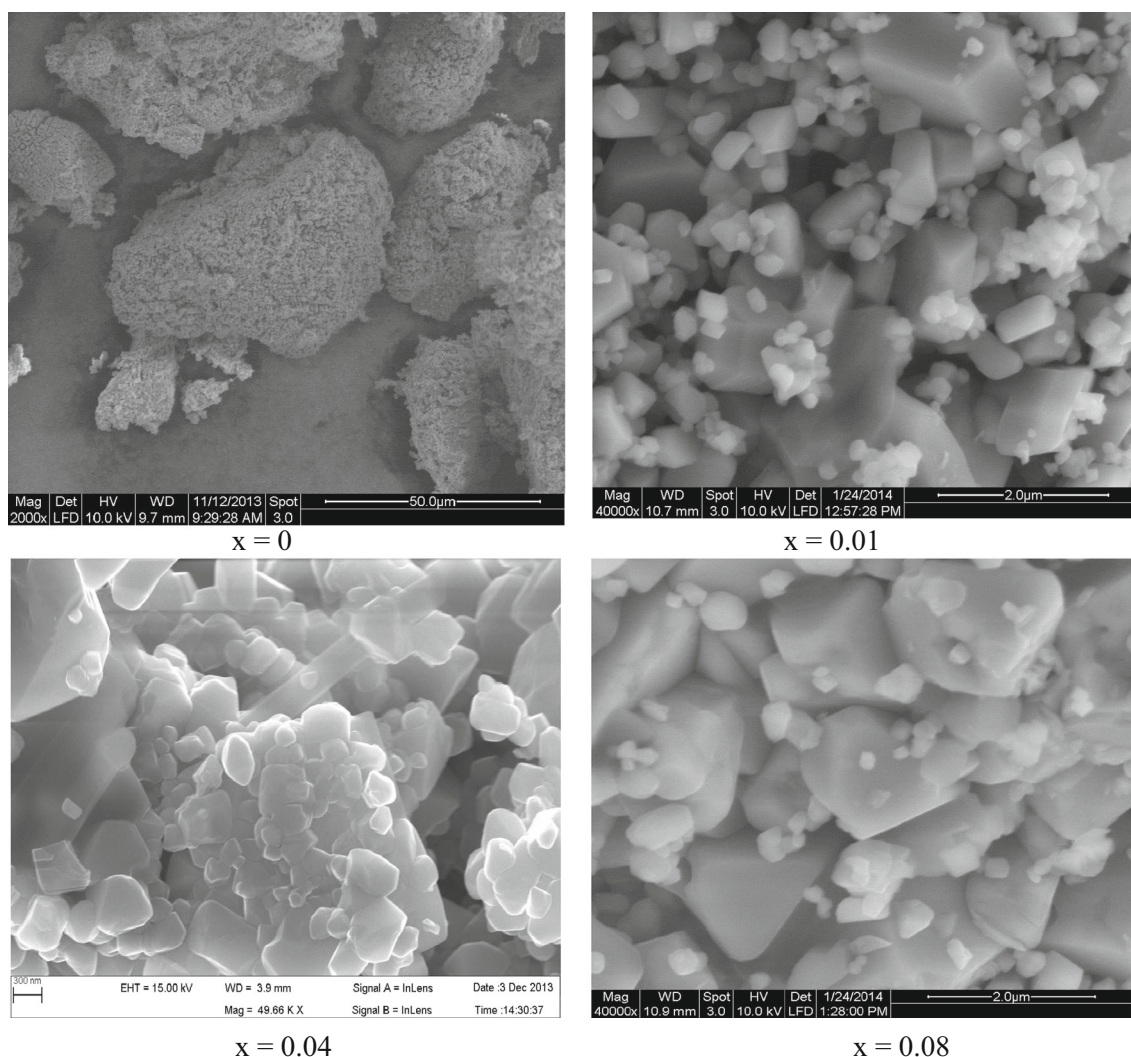


Fig. 2 Scanning electron micrographs obtained on $\text{Li}(\text{Mn}_{1/3}\text{Ni}_{1/3}\text{Co}_{1/3-x}\text{Na}_x)\text{O}_2$, $x = 0, 0.04, 0.08$, and 0.11 materials

size secondary particles create appropriately fine internal porous structure, the capillary action of which will facilitate proper wetting of the electrode material by the liquid electrolyte.

Further, the energy dispersive spectrum (EDS) obtained on these prepared materials show the presence of only Ni, Co, Mn, and O (Li cannot be detected by EDS) without any other impurity peaks. Moreover, the chemical compositions of all these materials are close to their stoichiometric ratios of the empirical formula. Specially, the atomic ratio of Ni/Mn/Co/Na was found to be approximately 7.58:7.36:6.02:0.46, 7.72:7.13:6.86:0.96, and 7.91:7.32:6.49:1.28 for $x = 0.04$, 0.08, and 0.11 composition, respectively. These results show that the chemical compositions of these synthesized materials are close to their stoichiometric ratios given by the chemical formula.

Hence, this study implies that the GNC process is a promising method to synthesize the phase pure $\text{Li}(\text{Ni}_{1/3}\text{Mn}_{1/3}\text{Co}_{1/3})\text{O}_2$ -based materials. The main advantage of this method is the possibility of synthesizing the desired highly crystalline material within a short calcination period compared to other previously investigated traditional synthesis methods [3–5, 8]. Furthermore, the resulting particle morphology of the present study consists of nano-scale primary particles with high surface area, softly agglomerated to form micron size secondary particles. Hence, this will be a much favorable particle morphology leading to higher electrochemical performance.

Figure 3 shows the thermogravimetric analysis (TG) of different materials. The TG curve shows that weight loss takes place in several steps. The weight loss step in the TG curve between room temperature and 100 °C is attributed to the evaporation of adsorbed water [1, 20]. Two weight loss steps between 100 and 400 °C resulting exothermic peaks around 195 and 285 °C can be clearly identified in Na-doped $\text{Li}(\text{Ni}_{1/3}\text{Mn}_{1/3}\text{Co}_{1/3})\text{O}_2$. TG curve of the $\text{Li}(\text{Ni}_{1/3}\text{Mn}_{1/3}\text{Co}_{1/3})\text{O}_2$ base material shows nearly steady weight loss over the temperature range between 100 and 400 °C as reported by other workers [1, 19]. Komaba et al. reported the irreversible phase transformation at temperature between 100 and 400 °C for Na-doped layered oxide by high-temperature XRD [20]. Therefore, exothermic peaks in $\text{Li}(\text{Ni}_{1/3}\text{Mn}_{1/3}\text{Co}_{1/3-x}\text{Na}_x)\text{O}_2$ materials may be related to irreversible phase transition [20]. All samples show weight loss between 550 and 800 °C. This stage corresponds to exothermic peak in differential thermogravimetric plots (dW/dT plots) at 700 °C for $x = 0.00$, 775 °C for $x = 0.04$, and 725 °C for $x = 0.08$ and 0.11 materials. Furthermore, weight losses occurring between 550 and 800 °C for $x = 0.04$, 0.08, and 0.11 materials are relatively lower (between 0.28 and 0.38%) compared to the weight loss of 1.21% that occurs in $\text{Li}(\text{Ni}_{1/3}\text{Mn}_{1/3}\text{Co}_{1/3})\text{O}_2$. The weight loss in this temperature range is attributed to the evolution of oxygen from the material

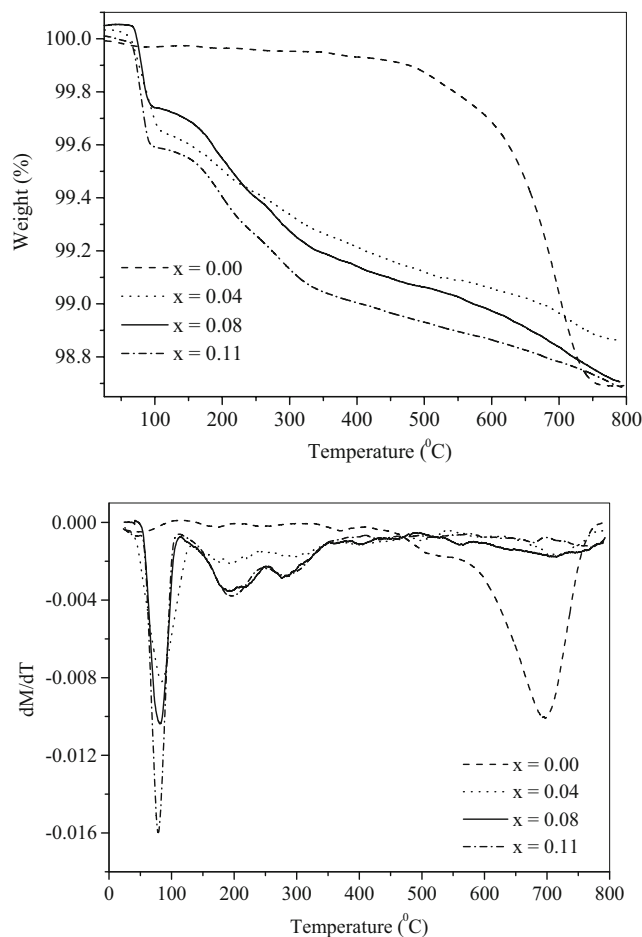


Fig. 3 Thermal gravimetric analysis (TGA) curves (*above*) and differential thermal analysis (DTA) curves obtained on $\text{Li}(\text{Ni}_{1/3}\text{Mn}_{1/3}\text{Co}_{1/3-x}\text{Na}_x)\text{O}_2$, $x = 0.00, 0.04, 0.08$, and 0.11 materials (*below*). The measurements were taken from 25 to 800 °C with a heating rate of 5 °C min^{-1} under nitrogen atmosphere

[1]. Therefore, the materials synthesized in this study by adding Na have better thermal stability at higher temperature than the base material.

Electrical conductivity of the prepared materials

The electrical conductivity was determined by the d.c. four probe technique, and Fig. 4 shows the temperature dependence of the conductivity of $\text{Li}(\text{Ni}_{1/3}\text{Mn}_{1/3}\text{Co}_{1/3-x}\text{Na}_x)\text{O}_2$ for $x = 0.00, 0.04, 0.08$, and 0.11 materials. In all these materials, the electrical conductivity increases exponentially with the measuring temperature indicating the semiconducting nature of these materials [15].

The room temperature (25 °C) electrical conductivity of $\text{Li}(\text{Ni}_{1/3}\text{Mn}_{1/3}\text{Co}_{1/3-x}\text{Na}_x)\text{O}_2$, $x = 0.00, 0.04, 0.08$, and 0.11 is given in Table 1. As given in Table 1, the room temperature electrical conductivity of $\text{Li}(\text{Ni}_{1/3}\text{Mn}_{1/3}\text{Co}_{1/3})\text{O}_2$ is in the order of 10^{-7} S cm^{-1} .

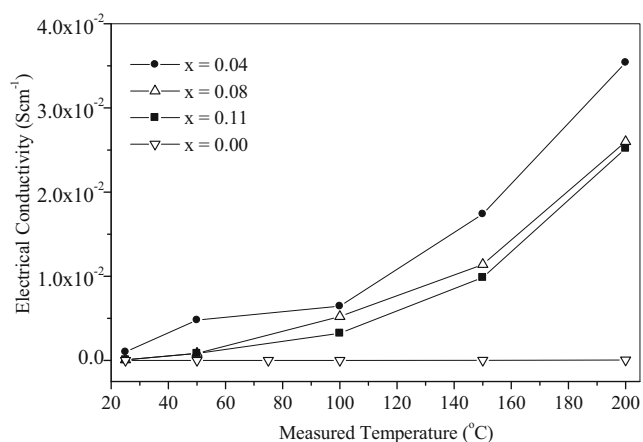


Fig. 4 The temperature dependence of the electrical conductivity of $\text{Li}(\text{Ni}_{1/3}\text{Mn}_{1/3}\text{Co}_{1/3-x}\text{Na}_x)\text{O}_2$, $x = 0.00, 0.04, 0.08,$ and 0.11 materials

However, for the Na-doped materials, the electrical conductivity is significantly higher, by a factor of about 10^4 for $x = 0.04$ compared to that of base material ($x = 0$). The electrical conductivity of semiconductors partially depends on the charge carrier concentration [21]. When Na^+ is added to $\text{Li}(\text{Ni}_{1/3}\text{Mn}_{1/3}\text{Co}_{1/3})\text{O}_2$, the amount of Ni^{+2} in Li layer may reduce, and in return, the $\text{Ni}^{+2}/\text{Ni}^{+3}$ in transition metal layer increases [3]. Hence, the increase of electrical conductivity due to Na^+ substitution in the present study may be attributed to the increased number of $\text{Ni}^{+3}/\text{Ni}^{+2}$ ions in the transition metal layer, which act as effective charge carriers to enhance the electrical conductivity.

So far in the present study, phase pure $\text{Li}(\text{Ni}_{1/3}\text{Mn}_{1/3}\text{Co}_{1/3-x}\text{Na}_x)\text{O}_2$ materials were successfully synthesized by the GNC process by calcining at comparatively lower temperature (900°C) and lower calcination period of 2 h. Moreover, it resulted a powder particle morphology more appropriate for LIB cathode application. Therefore, the present study has already possessed two main advantages on synthesizing Na-doped $\text{Li}(\text{Ni}_{1/3}\text{Mn}_{1/3}\text{Co}_{1/3-x}\text{Na}_x)\text{O}_2$ cathode materials. Firstly, it shows the possibility of addition of cheaper Na on behalf of highly expensive Co in $\text{Li}(\text{Ni}_{1/3}\text{Mn}_{1/3}\text{Co}_{1/3})\text{O}_2$ structure, which has not been reported yet to the authors' knowledge. Secondly, the production cost of the new material can be lowered significantly by the GNC process due to the considerable reduction of calcination temperature and period.

Electrochemical behavior of the prepared $\text{Li}(\text{Ni}_{1/3}\text{Mn}_{1/3}\text{Co}_{1/3})\text{O}_2$ base material

Galvanostatic cycling of coin cells fabricated with cathodes from synthesized $\text{Li}(\text{Ni}_{1/3}\text{Mn}_{1/3}\text{Co}_{1/3})\text{O}_2$ material and Li foil as the counter and reference electrode was carried out between 2.5 and 4.6 V at C/5 rate ($1\text{C} = 140\text{ mA g}^{-1}$). Figure 5 shows the first 10 cycles of charge/discharge profile of $\text{Li}(\text{Ni}_{1/3}\text{Co}_{1/3}\text{Mn}_{1/3})\text{O}_2$. The first cycle charge and discharge capacity is 212 and $187\text{ mA h}^{-1}\text{ g}^{-1}$, respectively. The initial

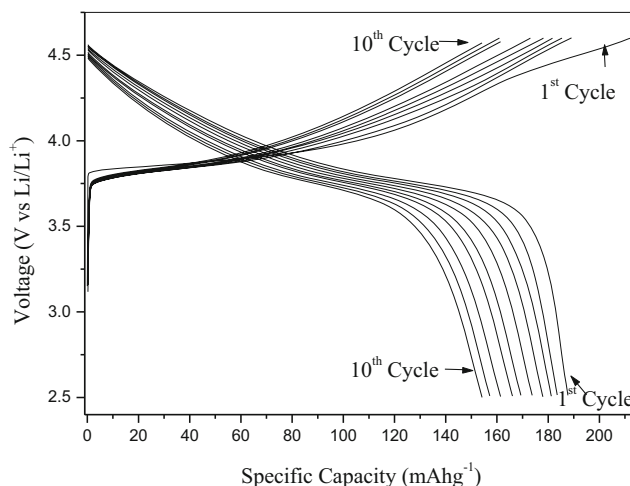


Fig. 5 First 10 cycles of the charge/discharge profile for $\text{Li}(\text{Ni}_{1/3}\text{Co}_{1/3}\text{Mn}_{1/3})\text{O}_2$ cathode at C/5 rate with a cut-off voltage of 2.5–4.6 V, at room temperature

irreversible capacity is thus $25\text{ mA h}^{-1}\text{ g}^{-1}$ with coulombic efficiency of 88.47%. During the second cycle, the irreversible capacity decreased to $5\text{ mA h}^{-1}\text{ g}^{-1}$ with coulombic efficiency of 97%. This could be attributed to the elimination of part of oxide ion vacancies and corresponding number of lithium sites, formation of SEI layer, and site reaction with electrolyte at very high operating voltage [4, 22]. As explained earlier, the SEM analysis (see Fig. 2) shows that the prepared $\text{Li}(\text{Ni}_{1/3}\text{Mn}_{1/3}\text{Co}_{1/3})\text{O}_2$ consists of quasi-spherical, micron size secondary particles formed by agglomerating nano-scale primary particles. Therefore, the high irreversible capacity loss reported here during the first cycle may be due to higher reactivity of the electrolyte with the large surface area resulting from nano-scale primary particles leading to formation of a thicker solid electrolyte interface [4].

In order to identify the electrochemical redox reaction which might occur during the charge and discharge processes, dQ/dV values (Q is the specific capacity and V is the voltage of the cell) were calculated from the numerical data obtained from Fig. 5 and the resulting dQ/dV vs. V plots are shown in Fig. 6. It can clearly be seen that this $\text{Li}(\text{Ni}_{1/3}\text{Co}_{1/3}\text{Mn}_{1/3})\text{O}_2$ material exhibits two oxidation peaks and one reduction peak during the first cycle. However, there is only one oxidation peak and one reduction peak observed in the second and tenth cycles. The sharp oxidation peaks at 3.8 V may be associated with the oxidation of Ni from Ni^{+2} to Ni^{+4} and oxidation of Co from Co^{+3} to Co^{+4} in order to compensate the charge balance in the lithium de-intercalation process [12]. During the discharge process, when lithium is intercalated back into the structure of the electrode, one reduction peak is distinguishable at around 3.7 V corresponding to the reduction of Ni^{+4} to Ni^{+2} and Co^{+4} to Co^{+3} [12]. This implies that the reversibility of the redox reaction is associated with the lithium intercalation and de-intercalation [6, 12]. Furthermore, the absence of oxidation or reduction peaks below 3.5 V in the charge

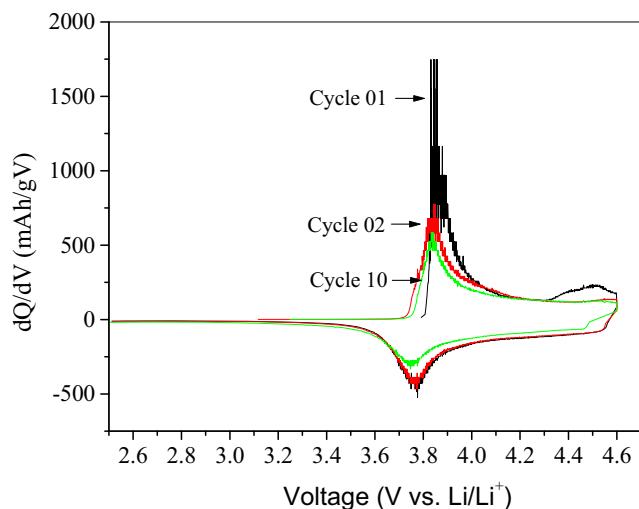


Fig. 6 Differential capacity versus voltage plots of $\text{Li}(\text{Ni}_{1/3}\text{Mn}_{1/3}\text{Co}_{1/3})\text{O}_2$ for the first, second, and tenth cycles

discharge profiles indicates that the Mn ions are electrochemically inactive [8].

The second oxidation peak appears at a potential above 4.5 V for the first cycle. However, there is no clear corresponding reduction peak for this process. This indicates the irreversibility for the reaction at this potential during the oxidation [12]. Differential capacity plots of the second and tenth cycle (see Fig. 5) imply that this oxidation peak is absent from the second cycle. The irreversible oxidation process occurring during the charging process at potentials above 4.5 V can be interpreted as the loss of oxygen with excess Li extraction from the layered structure, and the process is completed during the first charge [24].

Figure 7 shows rate capability of $\text{Li}(\text{Ni}_{1/3}\text{Co}_{1/3}\text{Mn}_{1/3})\text{O}_2$ with the rate ranging from C/5 to 1C rate at room temperature. The cell was first cycled at 0.2, 1, and 0.5 C for 3 cycles and back at 0.2 C. Subsequently, the cell was cycled at 0.2 C up to

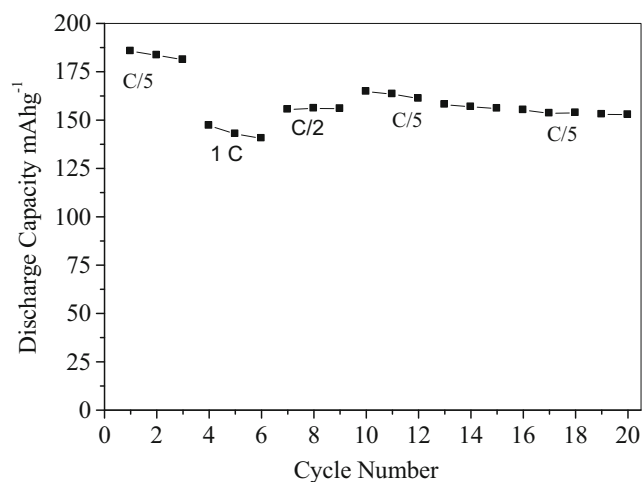


Fig. 7 The rate capability of $\text{Li}(\text{Ni}_{1/3}\text{Co}_{1/3}\text{Mn}_{1/3})\text{O}_2$ with the rate ranging from C/5 to 1C with a cut-off voltage of 2.5–4.6 V at room temperature

20 cycles. The $\text{Li}(\text{Ni}_{1/3}\text{Co}_{1/3}\text{Mn}_{1/3})\text{O}_2$ cathode material exhibits a high initial discharge capacity, at C/5 rate. The discharge capacity decreases from 187 to 181 $\text{mA h}^{-1} \text{g}^{-1}$ during the first 3 cycles at C/5 rate.

The discharge capacity decreases with increasing charge discharge rate, to 147 $\text{mA h}^{-1} \text{g}^{-1}$ when the cycle starts at 1 C rate and decreases further to 140 $\text{mA h}^{-1} \text{g}^{-1}$ within two consequent cycles. Then, the discharge capacity increases to 155 $\text{mA h}^{-1} \text{g}^{-1}$ with the increasing of C rate to C/2, and discharge capacity is retained at a constant value. Again, the discharge capacity increased to 164 $\text{mA h}^{-1} \text{g}^{-1}$ at the 10th cycle since the current decreases to C/5. The tested cell exhibits 84% of capacity to its second discharge after the 20th cycle. This implies that a significant rate capability of $\text{Li}(\text{Ni}_{1/3}\text{Co}_{1/3}\text{Mn}_{1/3})\text{O}_2$ results due to the ordered crystal structure and optimum microstructure as already explained by the XRD and SEM analysis of the present study [6, 7, 11].

Samarasinghe et al. had synthesized phase pure $\text{Li}(\text{Ni}_{1/3}\text{Co}_{1/3}\text{Mn}_{1/3})\text{O}_2$ by the Pechini method and by calcination at 900 °C for 4 h [2]. The microstructure of this material was a sponge-like agglomerate with large primary particles (0.8–1 μm). Further, the cell testing had given an initial discharge capacity of $\sim 160 \text{ mA h}^{-1} \text{g}^{-1}$ at C/5 rate between 3 and 4.5 V. In contrast, the $\text{Li}(\text{Ni}_{1/3}\text{Co}_{1/3}\text{Mn}_{1/3})\text{O}_2$ synthesized by GNC method in the present study gives an initial discharge capacity of $\sim 187 \text{ mA h}^{-1} \text{g}^{-1}$ at C/5 rate between 2.5 and 4.6 V, showing considerable improvement in rate capability as discussed above. This may be attributed to the higher surface area resulted from agglomerating nano-scale primary particles to form secondary micron size particles. Therefore, $\text{Li}(\text{Ni}_{1/3}\text{Co}_{1/3}\text{Mn}_{1/3})\text{O}_2$ material synthesized by GNC process in the present study resulted powders with microstructure more suitable for LIB cathode and ended up with improved electrochemical performance.

Electrochemical behavior of Na-doped $\text{Li}(\text{Ni}_{1/3}\text{Mn}_{1/3}\text{Co}_{1/3-x}\text{Na}_x)\text{O}_2$ materials

Initial charge-discharge curves of $\text{Li}(\text{Ni}_{1/3}\text{Mn}_{1/3}\text{Co}_{1/3-x}\text{Na}_x)\text{O}_2$ ($x = 0.00, 0.04, 0.08, 0.11$) at C/5 rate with a cut-off voltage of 2.5–4.6 V at room temperature are shown in Fig. 8. All these cells exhibited very smooth and consistent charge/discharge curves and a voltage profile similar to those reported in the literature [3]. Further, it is clearly seen that the discharge capacity decreases monotonically with the increase of Na content. The initial discharge capacity of $\text{Li}(\text{Ni}_{1/3}\text{Mn}_{1/3}\text{Co}_{1/3-x}\text{Na}_x)\text{O}_2$, $x = 0.00, 0.04, 0.08$, and 0.11 are 187.7, 182.6, 111.8, and 27.2 $\text{mA h}^{-1} \text{g}^{-1}$, respectively (Table 2). Here, the addition of Na at a higher concentration ($x = 0.11$) leads to a drop in the discharge capacity to 27 $\text{mA h}^{-1} \text{g}^{-1}$. Previous studies on Na-substituted $\text{Li}_{1-x}\text{Na}_x(\text{Ni}_{1/3}\text{Mn}_{1/3}\text{Co}_{1/3})\text{O}_2$ reported the decreases of initial discharge capacity with the increasing of Na substitution (175.8 $\text{mA h}^{-1} \text{g}^{-1}$ for $x = 0.00$,

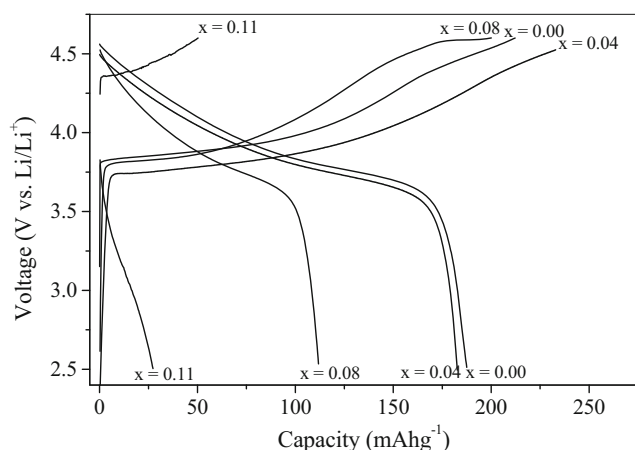


Fig. 8 Initial charge/discharge curves of the $\text{Li}(\text{Ni}_{1/3}\text{Mn}_{1/3}\text{Co}_{1/3-x}\text{Na}_x)\text{O}_2$ ($x = 0.00, 0.04, 0.08, 0.11$) at $C/5$ rate with a cut-off voltage of 2.5–4.6 V, at room temperature

174.0 $\text{mA h}^{-1} \text{g}^{-1}$ for 0.001, $x = 170.9 \text{ mA h}^{-1} \text{g}^{-1}$ for 0.01, 172.7 $\text{mA h}^{-1} \text{g}^{-1}$ for $x = 0.03$ and 166.5 $\text{mA h}^{-1} \text{g}^{-1}$ for $x = 0.03$ between 2.7 and 4.4 V under current density of 16 mA g^{-1} [9]. Another study showed higher initial discharge capacity Na-doped $\text{Li}_{0.95}\text{Na}_{0.05}\text{Ni}_{1/3}\text{Co}_{1/3}\text{Mn}_{1/3}\text{O}_2$ (250.5 $\text{mA h}^{-1} \text{g}^{-1}$) than $\text{Li}(\text{Ni}_{1/3}\text{Mn}_{1/3}\text{Co}_{1/3})\text{O}_2$ (155.4 $\text{mA h}^{-1} \text{g}^{-1}$) under current density of 27 mA g^{-1} in the potential range of 2.0–4.5 V [3]. Qiu et al. reported that the discharge capacity of Na-substituted $\text{Li}_{1.2-x}\text{Na}_x\text{Ni}_{0.13}\text{Co}_{0.13}\text{Mn}_{0.54}\text{O}_2$ system increases compared to the unsubstituted system from $x = 0.005$ to $x = 0.02$ due to the increase in d-spacing with the substitution of Li^+ sites by a small amount of Na^+ ions [8]. Further, they reported that at $x = 0.05$, the initial discharge capacity was equal to the nonsubstituted ($x = 0.00$) material. Qiu et al. reported that

Table 2 The first, second, and tenth cycle charge-discharge data of $\text{Li}(\text{Ni}_{1/3}\text{Mn}_{1/3}\text{Co}_{1/3-x}\text{Na}_x)\text{O}_2$, $x = 0.04, 0.08, \text{ and } 0.11$

x in $\text{Li}(\text{Ni}_{1/3}\text{Mn}_{1/3}\text{Co}_{1/3-x}\text{Na}_x)\text{O}_2$	Cycle no.	Charge capacity (mAh g^{-1})	Discharge capacity (mAh g^{-1})	Columbic efficiency (%)	Irreversible capacity (mAh g^{-1})
0.00	1	212.2	187.7	88.5	24.4
	2	189.1	183.5	97.0	5.59
	10	157.4	154.1	97.9	3.2
0.04	1	232.9	182.6	78.4	50.2
	2	199.6	184.2	92.2	15.4
	10	161.9	159.9	98.7	2.0
0.08	1	200.0	111.8	55.8	88.2
	2	113.4	105.9	93.4	7.4
	10	92.0	91.7	99.7	0.2
0.11	1	50.3	27.2	54.1	23.0
	2	34.2	28.6	83.6	5.5
	10	27.9	26.3	94.1	1.6

the discharge capacity of Na-substituted $\text{Li}_{1.2-x}\text{Na}_x\text{Ni}_{0.13}\text{Co}_{0.13}\text{Mn}_{0.54}\text{O}_2$ system increases compared to the unsubstituted system from $x = 0.005$ to $x = 0.02$ due to the increase in d-spacing with the substitution of Li^+ sites by a small amount of Na^+ ions [8]. It has earlier been reported that the differences in the radii of the Na^+ and Li^+ cations lead to occupation of Li in the transition metal layer in the precursor [23]. Therefore, reduction of discharge capacity with increase in Na concentration may be due to a combination of decreasing lithium content in the Li layer [23] and the inhabitation of lithium diffusion due to occupation of high amount of Na in the lithium layer [8].

Table 2 summarizes the results of the charge/discharge study conducted using the prepared $\text{Li}(\text{Ni}_{1/3}\text{Mn}_{1/3}\text{Co}_{1/3-x}\text{Na}_x)\text{O}_2$ ($x = 0.00, 0.04, 0.08, \text{ and } 0.11$) of the present study. Initial irreversible capacity of $x = 0$ materials is 24 $\text{mA h}^{-1} \text{g}^{-1}$ with columbic efficiency of 88.47%. The first cycle irreversible capacity of $x = 0.04, 0.08, \text{ and } 0.11$ materials is 50, 88, and 23.05 $\text{mA h}^{-1} \text{g}^{-1}$, respectively, with the columbic efficiency of 78.4, 55.87, and 54.16%. This implies that the irreversible capacity during the first cycle of Na-doped materials is higher than that of the unsubstituted ($x = 0$) material and columbic efficiency decreases with increasing Na level in $\text{Li}(\text{Ni}_{1/3}\text{Mn}_{1/3}\text{Co}_{1/3-x}\text{Na}_x)\text{O}_2$.

This significant increase in irreversible capacity in the first cycle may be caused by several factors such as (i) the de-intercalated lithium cannot re-intercalate into the host because the crystal lattice of the host is slightly changed during the first cycle [4], (ii) irreversible loss of oxygen from the lattice [22], and (iii) irreversible charge consumed by the electrolyte decomposition during the first cycle [4]. Those effects are related to the crystal structure and microstructure of the cathode material. The SEM micrographs given in Fig. 2 show the formation of nano-scale primary particles resulting higher internal surface area. Size of the primary particles increases with the increasing level of Na substitution. A large particle size might cause higher polarization and affect the Li^+ ion diffusion in solid phase resulting lowering the columbic efficiency with increasing particle size [11]. This might be one reason for the considerably higher irreversible capacity losses in the present case. Furthermore, inhabitation of lithium diffusion due to occupation of high amount of Na in the lithium layer [8] and occupation of Li in the precursor in transition metal layer might be other reasons for the increase in irreversible capacity during first cycle with the increase level of Na doping. However, reasons for the higher irreversible capacity loss due to the increase of Na addition are not well understood yet.

In order to identify the electrochemical redox reactions, which might occur during the charge and discharge process, dQ/dV values were calculated from the numerical data observed in Fig. 8, and the corresponding dQ/dV vs. V plots are presented in Fig. 9a, b. It can be clearly seen that the $\text{Li}(\text{Ni}_{1/3}\text{Mn}_{1/3}\text{Co}_{1/3-x}\text{Na}_x)\text{O}_2$ with $x = 0.04$ and 0.08 exhibits

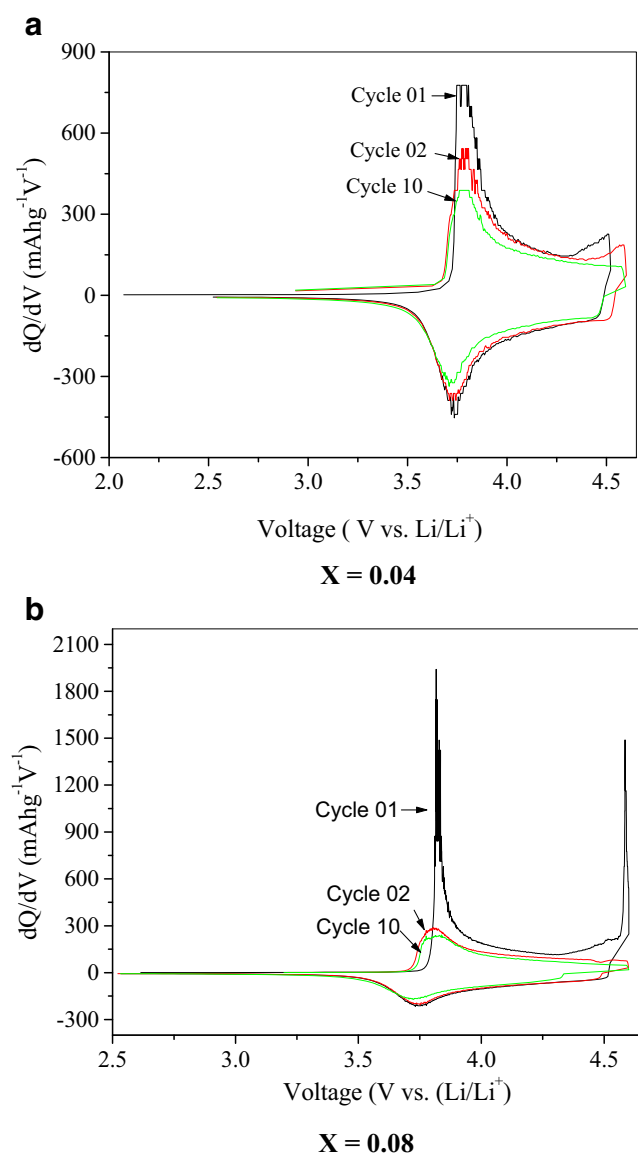


Fig. 9 Differential capacity versus voltage for $\text{Li}(\text{Ni}_{1/3}\text{Mn}_{1/3}\text{Co}_{1/3-x}\text{Na}_x)\text{O}_2$ $x = 0.04$ (a) and 0.08 (b) for the first, second, and tenth cycles

two oxidation peaks and one reduction peak during the first cycle. Sharp oxidation peaks, at 3.77 V for $x = 0.04$ and 3.8 V for $x = 0.08$, are observed from these differential capacity plots of each cycle. This peak may be associated with Ni oxidation from Ni^{+2} to Ni^{+4} and Co oxidation from Co^{+3} to Co^{+4} compensating the charge balance due to lithium de-intercalation [24]. During the discharge process, when lithium is inserted back into the structure of the electrode, one reduction peak is distinguishable at 3.7 V corresponding to the reduction of Ni^{+4} to Ni^{+2} and Co^{+4} to Co^{+3} [24]. This implies the reversibility of the redox reaction associated with the lithium intercalation and de-intercalation [24, 25]. Previous studies reported that the Na doping may activate the Mn in the layered transition metal oxides contributing additional discharge capacity [8]. However, the absence of oxidation or reduction peaks below

3.5 V in the differential capacity plots of $x = 0.04$ and $x = 0.08$ in the present study indicates that the Mn ions are electrochemically inactive.

As seen in Fig. 9, the second oxidation peak appears around 4.5 V for the first cycle. However, there is no obvious corresponding reduction peak for this process, indicating the irreversibility of the reaction at this potential during the oxidation. The irreversible oxidation process occurring during the charging process at potential around 4.5 V can be interpreted with the loss of oxygen with excess Li extraction from the layered structure, and the process is completed during the first charge [22]. The second oxidation peak at potential around 4.5 V in the first and second cycle charging process of $\text{Li}(\text{Ni}_{1/3}\text{Mn}_{1/3}\text{Co}_{1/3-x}\text{Na}_x)\text{O}_2$, $x = 0.04$ results from the irreversible capacity of 50 and $15\text{ mA h}^{-1}\text{ g}^{-1}$ for the first and second cycles, respectively. However, this peak had disappeared from the third cycle. Intensity of the second oxidation peak is very high in $x = 0.08$ material compared to the $x = 0.00$ and 0.04 materials. This suggests that there is a very high first cycle irreversible capacity loss ($88.2\text{ mA h}^{-1}\text{ g}^{-1}$) in $x = 0.08$ material. However, the differential capacity plots of the second and tenth cycles indicate the absence of this oxidation peak from the second cycle.

Although the $\text{Li}(\text{Ni}_{1/3}\text{Mn}_{1/3}\text{Co}_{1/3})\text{O}_2$ ($x = 0$) material (as discussed under “Electrochemical behavior of the prepared $\text{Li}(\text{Ni}_{1/3}\text{Mn}_{1/3}\text{Co}_{1/3})\text{O}_2$ base material” section) delivered the highest initial discharge capacity of $187.73\text{ mA h}^{-1}\text{ g}^{-1}$ at the C/5 rate, it showed gradual fading of capacity down to $154\text{ mA h}^{-1}\text{ g}^{-1}$ after 10 cycles (see Table 2). In contrast, the initial discharge capacity of $\text{Li}(\text{Ni}_{1/3}\text{Mn}_{1/3}\text{Co}_{1/3-x}\text{Na}_x)\text{O}_2$, $x = 0.04$ material was $182.6\text{ mA h}^{-1}\text{ g}^{-1}$, and its discharge capacity fades only to $159.9\text{ mA h}^{-1}\text{ g}^{-1}$ after 10 cycles. This shows a slightly improved cycle performance with the Na doping. Also, the Na-doped $\text{Li}(\text{Ni}_{1/3}\text{Mn}_{1/3}\text{Co}_{1/3-x}\text{Na}_x)\text{O}_2$, $x = 0.08$ material shows 94.3% capacity retention of its second cycle discharge capacity. The improved cycle performance of the Na-doped materials could be ascribed to the combination of several factors such as (i) increase of c -parameter with the substitution of Li^{+} by a small amount of Na^{+} ions, which is beneficial for the Li^{+} diffusion, and (ii) reduction of degree of cation mixing as evident by XRD data [3, 8, 9]. The enhanced cycle performance implies the advantage of substitution of low-cost Na for costly Co in low level doping to $\text{Li}(\text{Ni}_{1/3}\text{Mn}_{1/3}\text{Co}_{1/3})\text{O}_2$.

The $x = 0.04$ material synthesized by GNC exhibits a discharge capacity much closer to that of the base material ($x = 0$) and shows an improved electrochemical performance. In this study, Co was substituted by Na to explore the possibility of lowering the amount of expensive Co and get the advantage of high discharge capacity induced by the Na doping as proposed by previously with $\text{Li}_{1-x}\text{Na}_x(\text{Ni}_{1/3}\text{Co}_{1/3}\text{Mn}_{1/3})\text{O}_2$ materials [3, 8, 9]. Eventhough the initial discharge capacity of $\text{Li}(\text{Ni}_{1/3}\text{Mn}_{1/3}\text{Co}_{1/3-x}\text{Na}_x)\text{O}_2$ $x = 0.04$ material synthesized in

this study ($182 \text{ mA h}^{-1} \text{ g}^{-1}$ between 2.5 and 4.6 V) is considerably lower to that of $\text{Li}_{0.95}\text{Na}_{0.05}\text{Ni}_{1/3}\text{Co}_{1/3}\text{Mn}_{1/3}\text{O}_2$ ($250 \text{ mA h}^{-1} \text{ g}^{-1}$ between 2.0 and 4.5 V) [3], it is still comparable with the $\text{Li}_{0.999}\text{Na}_{0.001}\text{Ni}_{1/3}\text{Co}_{1/3}\text{Mn}_{1/3}\text{O}_2$ ($174.0 \text{ mA h}^{-1} \text{ g}^{-1}$ between 2.7 and 4.4 V) [10]. Therefore, this study shows a new direction of Na substitution to $\text{Li}(\text{Ni}_{1/3}\text{Mn}_{1/3}\text{Co}_{1/3})\text{O}_2$ system.

Na-substituted $\text{Li}_{1-x}\text{Na}_x(\text{Ni}_{1/3}\text{Mn}_{1/3}\text{Co}_{1/3})\text{O}_2$ material synthesized by molten salts method showed initial discharge capacity of $175.8 \text{ mA h}^{-1} \text{ g}^{-1}$ for $x = 0.00$, $174.0 \text{ mA h}^{-1} \text{ g}^{-1}$ for $x = 0.001$, $170.9 \text{ mA h}^{-1} \text{ g}^{-1}$ for $x = 0.01$, $172.7 \text{ mA h}^{-1} \text{ g}^{-1}$ for $x = 0.03$ and $166.5 \text{ mA h}^{-1} \text{ g}^{-1}$ for $x = 0.05$ between 2.7 and 4.4 V under current density of 16 mA g^{-1} [10].

Altogether, an alternative cathode material prepared by replacing a part of costly Co by cheaper Na, and possessing higher electrical conductivity while preserving the appropriate layered structure, both of which are decisive economic and materials factors for the LIB cathode, is generally interesting. Specially, the $\text{Li}(\text{Ni}_{1/3}\text{Mn}_{1/3}\text{Co}_{1/3-x}\text{Na}_x)\text{O}_2$ $x = 0.04$ cathode material investigated in this study showed a comparable initial discharge capacity together with improved capacity retention compared to those of the $\text{Li}(\text{Ni}_{1/3}\text{Mn}_{1/3}\text{Co}_{1/3})\text{O}_2$ base material, which in turn already a better competitor to the presently used state-of-the-art LiCoO_2 cathode in LIB [1, 2, 4–7]. Therefore, $\text{Li}(\text{Ni}_{1/3}\text{Mn}_{1/3}\text{Co}_{1/3-x}\text{Na}_x)\text{O}_2$ $x = 0.04$ material, synthesized by the GNC technique is cost-effective and performance-enhanced cathode material for LIB.

Conclusions

Phase-pure $\text{Li}(\text{Ni}_{1/3}\text{Mn}_{1/3}\text{Co}_{1/3-x}\text{Na}_x)\text{O}_2$ ($x = 0.00, 0.04, 0.08,$ and 0.11) material, formed by the softly agglomerated nanoscale primary particles, was successfully synthesized by the glycine-nitrate combustion (GNC) process at a comparatively low temperature of $900 \text{ }^\circ\text{C}$ under a shorter calcination time of 2 h. The X-ray diffraction study further elaborated an increase in c -parameter in the $x = 0.04$ material. This could be beneficial for the Li diffusion between oxygen layers and reduction of degree of cation mixing. The electrical conductivity of the Na-doped materials significantly increases by a factor of 10^4 for $x = 0.04$ and 10^2 for $x = 0.08$ and 0.11 compared to that of the $\text{Li}(\text{Ni}_{1/3}\text{Mn}_{1/3}\text{Co}_{1/3})\text{O}_2$ base material (with $2.06 \times 10^{-7} \text{ S cm}^{-1}$ at $25 \text{ }^\circ\text{C}$). The increased number of $\text{Ni}^{3+}/\text{Ni}^{2+}$ ions, which act as charge carrier due to the reduction of Ni^{2+} in Li layer by Na substitution, may be the reason to enhance the conductivity. The $\text{Li}(\text{Ni}_{1/3}\text{Mn}_{1/3}\text{Co}_{1/3})\text{O}_2$ material showed initial discharge capacity of $187 \text{ mA h}^{-1} \text{ g}^{-1}$ with $25 \text{ mA h}^{-1} \text{ g}^{-1}$ irreversible capacity loss and 88.47% columbic efficiency at C/5 rate with a cut-off voltage of 2.5–4.6 V at $25 \text{ }^\circ\text{C}$. More interestingly, the $\text{Li}(\text{Ni}_{1/3}\text{Mn}_{1/3}\text{Co}_{1/3-x}\text{Na}_x)\text{O}_2$, ($x = 0.04$) cathode showed a comparable initial discharge capacity but interestingly with substantially improved capacity

retention. This could be resulted due to decreased cation mixing and an increased Li slab dimension in this Na-doped material compared to $\text{Li}(\text{Ni}_{1/3}\text{Mn}_{1/3}\text{Co}_{1/3})\text{O}_2$ base material. Altogether, this study showed the potentiality of $\text{Li}(\text{Ni}_{1/3}\text{Mn}_{1/3}\text{Co}_{1/3}\text{Na}_x)\text{O}_2$ materials synthesized by glycine nitrate combustion method with promising particle morphology and electrochemical behavior for the rechargeable Li-ion battery cathode.

Acknowledgements Financial assistance by the Human Resources Development (HRD) program of the Higher Education for Twenty First Century (HETC) project of Ministry of Higher Education, Sri Lanka is acknowledged.

References

- Kabi S, Ghosh A (2013) Microstructure of $\text{Li}(\text{Mn}_{1/3}\text{Ni}_{1/3}\text{Co}_{1/3})\text{O}_2$ cathode material for lithium ion battery: dependence of crystal structure on calcination and heat-treatment temperature. *Mater Res Bull* 48:3405. doi:10.1016/j.materresbull.2013.05.012
- Samarasingha P, Tran-Nguyen D-H, Behm M, Wijayasinghe A (2008) $\text{Li}(\text{Mn}_{1/3}\text{Ni}_{1/3}\text{Co}_{1/3})\text{O}_2$ synthesized by the Pechini method for the positive electrode in li-ion batteries: material characteristics and electrochemical behaviour. *Electrochim Acta* 53:7995. doi:10.1016/j.electacta.2008.06.003
- Gong C, Lv W, Qu L, Bankole OE, Li G, Zhang R, Hu M, Lei L (2014) Syntheses and electrochemical properties of layered $\text{Li}_{0.95}\text{Na}_{0.05}\text{Ni}_{1/3}\text{Co}_{1/3}\text{Mn}_{1/3}\text{O}_2$ and $\text{Li}(\text{Mn}_{1/3}\text{Ni}_{1/3}\text{Co}_{1/3})\text{O}_2$. *J Power Sources* 247:151. doi:10.1016/j.jpowsour.2013.08.081
- Zhang S (2007) Characterization of high tap density $\text{Li}(\text{Mn}_{1/3}\text{Ni}_{1/3}\text{Co}_{1/3})\text{O}_2$ cathode material synthesized via co-precipitation. *Electrochim Acta* 52(25):7337. doi:10.1016/j.electacta.2007.06.015
- Yabuuchi N, Ohzuku T (2003) Novel lithium insertion material of $\text{Li}(\text{Mn}_{1/3}\text{Ni}_{1/3}\text{Co}_{1/3})\text{O}_2$ for advanced lithium-ion batteries. *J Power Sources* 119–121:171. doi:10.1016/S0378-7753(03)00173-3
- Nam K-W, Yoon W-S, Yang X-Q (2009) Structural changes and thermal stability of charged $\text{LiNi}_{1/3}\text{Co}_{1/3}\text{Mn}_{1/3}\text{O}_2$ cathode material for li-ion batteries studied by time-resolved XRD. *J Power Sources* 189:515. doi:10.1016/j.jpowsour.2008.10.130
- Oljaca M, Blizanac B, Pasquier AD, Sun Y, Bontchev R (2014a) Novel $\text{Li}(\text{Mn}_{1/3}\text{Ni}_{1/3}\text{Co}_{1/3})\text{O}_2$ cathode morphologies for high power li ion-batteries. *J Power Sources* 248:729. doi:10.1016/S0378-7753(03)00173-3
- Santhanam R, Rambabu B (2010) High rate cycling performance of $\text{Li}_{1.05}\text{Ni}_{1/3}\text{Co}_{1/3}\text{Mn}_{1/3}\text{O}_2$ materials prepared by sol-gel and co-precipitation methods for lithium-ion batteries. *J Power Sources* 195:4313. doi:10.1016/j.jpowsour.2010.01.016
- Qiu B, Wang J, Xia Y, Liu Y, Qin L, Yao X, Liu Z (2012) Effects of Na^+ contents on electrochemical properties of $\text{Li}_{1.2}\text{Ni}_{0.13}\text{Co}_{0.13}\text{Mn}_{0.54}\text{O}_2$ cathode materials. *J Power Sources* 240:530. doi:10.1016/j.jpowsour.2013.04.047
- Chen Z, Xie T, Li L, Xu M, Zhu H, Wang W (2014) Characterization of Na-substituted $\text{LiNi}_{1/3}\text{Co}_{1/3}\text{Mn}_{1/3}\text{O}_2$ cathode materials for lithium-ion battery. *Ionics* 20:629. doi:10.1007/s11581-013-1022-y
- He W, Yuan D, Qian J, Ai X, Yang H, Cao Y (2013) Enhanced high-rate capability and cycling stability of Na-stabilized layered $\text{Li}_{1.2}\text{Ni}_{0.13}\text{Co}_{0.13}\text{Mn}_{0.54}\text{O}_2$ cathode materials. *J Mater Chem A* 1: 11397. doi:10.1039/c3ta12296d

12. Liu J, Chen H, Xie J, Sun Z, Wu N, Wu B (2014) Electrochemical performance studies of li-rich cathode materials with different primary particle sizes. *J Power Sources* 251:208. doi:10.1016/j.jpowsour.2013.11.055
13. Wu F, Wang M, Su Y, Bao L, Chen S (2010a) A novel method for synthesis of layered $\text{Li}(\text{Mn}_{1/3}\text{Ni}_{1/3}\text{Co}_{1/3})\text{O}_2$ as cathode material for lithium-ion battery. *J Power Sources* 195:2362. doi:10.1016/j.jpowsour.2009.10.043
14. Samarasinghe PB, Wijayasinghe A, Bhem M, Dissanayake L, Lindhberg G (2014) Development of cathode materials for lithium ion rechargeable batteries based on the system $\text{Li}(\text{Ni}_{1/3}\text{Mn}_{1/3}\text{Co}_{1/3-x}\text{M}_x)\text{O}_2$ ($\text{M} = \text{Mg, Fe, Al}$ and $x = 0.00$ to 0.33). *Solid State Ionics* 268:226. doi:10.1016/j.ssi.2014.07.012
15. Lee J-W, Lee J-H, Viet TT, Lee J-Y, Kim J-S, Lee C-H (2010) Synthesis of $\text{Li}(\text{Mn}_{1/3}\text{Ni}_{1/3}\text{Co}_{1/3})\text{O}_2$ cathode materials by using a supercritical water method in a batch reactor. *Electrochim Acta* 55:3015. doi:10.1016/j.electacta.2009.12.080
16. Wijayasinghe A, Bergman B, Lagergren C (2006) LiFeO_2 – LiCoO_2 – NiO materials for molten carbonate fuel cell cathodes. Part I: powder synthesis and material characterization. *Solid State Ionics* 177:165. doi:10.1016/j.ssi.2005.10.018
17. Patoux S, Doeff MM (2004) Direct synthesis of $\text{Li}(\text{Mn}_{1/3}\text{Ni}_{1/3}\text{Co}_{1/3})\text{O}_2$ from nitrate precursors. *Electrochem Commun* 6:767. doi:10.1016/j.elecom.2004.05.024
18. Chick LA, Pederson LR, Maupin GD, Bates JL, Thomas LE, Exarhos GJ (1990) Glycine-nitrate combustion synthesis of oxide ceramic powders. *Mater Lett* 10(2):7. doi:10.1016/0167-577X(90)90003-5
19. Wilcox J, Patoux S, Doeff M (2009) Structure and electrochemistry of $\text{LiNi}_{1/3}\text{Co}_{1/3-y}\text{M}_y\text{Mn}_{1/3}\text{O}_2$ ($\text{M} = \text{Ti, Al, Fe}$) positive electrode materials. *J Electrochemical Society* 156(3):A192. doi:10.1149/1.3056109
20. Komaba S, Croguennec L, Tournadre F, Willmann P, Delmas C (2013) Thermal behavior of the layered oxide $\text{Li}_{2/3}\text{Co}_{2/3}\text{Mn}_{1/3}\text{O}_2$ Obtained by Ion Exchange from the P2-Type $\text{Na}_{2/3}\text{Co}_{2/3}\text{Mn}_{1/3}\text{O}_2$ Phase 2013. *J Phys Chem C* 117(7):3264. doi:10.1021/jp310417q
21. Shackelford JF (2005) Semiconductor materials, introduction to materials science for engineers, Vol 17. Ch. 6. Pearson Education, Inc., 17, p 622
22. Shi SJ, Tu JP, Tang YY, Yu YX, Zhang YQ, Wang XL, Gu CD (2013) Combustion synthesis and electrochemical performance of $\text{Li}[\text{Li}_{0.2}\text{Mn}_{0.54}\text{Ni}_{0.13}\text{Co}_{0.13}]\text{O}_2$ with improved rate capability. *J Power Sources* 228:14. doi:10.1016/j.jpowsour.2012.11.091
23. Kim D, Kang S-H, Balasubramanian M, Johnson CS (2010) High-energy and high-power li-rich nickel manganese oxide electrode materials. *Electrochem Commun* 12:1618
24. Wu F, Wang M, Su Y, Bao L, Chen S (2010b) A novel method for synthesis of layered $\text{LiNi}_{1/3}\text{Mn}_{1/3}\text{Co}_{1/3}\text{O}_2$ as cathode material for lithium-ion battery. *J Power Sources* 195:2362. doi:10.1016/j.jpowsour.2009.10.043
25. Oljaca M, Bliznac B, Pasquier AD, Sun Y, Bontchev R, Suszko A, Wall R, Koehlert K (2014b) Novel $\text{Li}(\text{Ni}_{1/3}\text{Co}_{1/3}\text{Mn}_{1/3})\text{O}_2$ cathode morphologies for high power li-ion battery. *J Power Sources* 248:729. doi:10.1016/j.jpowsour.2013.09.102